GeoScienceWorld
Lithosphere
Volume 2022, Article ID 7800281, 14 pages
https://doi.org/10.2113/2022/7800281

Lithosphere

Research Article

Tectonic Features of the Wufeng–Longmaxi Formation in the Mugan Area, Southwestern Sichuan Basin, China, and Implications for Shale Gas Preservation

Qiao Wang,[1] **Jian Yang**,[1] **Hu Wang**,[2] **Qian Yu**,[1] **Shibin Xia**,[1] **Guozhong Liao**,[1] **Wei Zhang**,[1] **Hua Li**,[1] **and Hui Gao**[1]

[1]*China Geological Survey, Chengdu Centre, Chengdu 610081, China*
[2]*Faculty of Geosciences and Environmental Engineering, Southwest Jiaotong University, Chengdu 611756, China*

Correspondence should be addressed to Qiao Wang; 540363176@qq.com, Jian Yang; yangjian831210@yeah.net, and Hu Wang; wanghu9905@126.com

Received 21 March 2022; Accepted 2 July 2022; Published 21 July 2022

Academic Editor: Shuangpo Ren

Shale gas resources in mainland China and its commercial exploitation has been widely focused on the Wufeng–Longmaxi Formation organic-matter-rich shale in the Sichuan Basin. However, whether southwestern margin of the Sichuan Basin can produce high-quality shale gas has not been well resolved, which might be related to the poor understanding of the relationship between Cenozoic tectonic deformation and shale gas preservation. To answer the aforementioned scientific question, we conducted a detailed work in the Mugan area to show geologic structures and gas contents in the area through seismic profiles and geochemistry analysis. Specifically, the stable Mugan syncline shows a high gas content (>2.6 m^3/t measured at three boreholes D1, D2, and D3), whereas its periphery presents a poor gas content (about 0.6 m^3/t measured at two boreholes X1 and Y1). Moreover, oblique fracture density and dissolved pores are much higher at boreholes X1 and Y1 than that at the other three boreholes. We propose an opposite-verging thrust fault model to explain the different gas contents and tectonic features in the Mugan area, which might indicate that regions in the southwestern Sichuan Basin with similar tectonic and stratigraphic characteristics as those in the Mugan syncline are likely to produce high-yield shale gas. This finding provides new insights into the exploration theory of shale gas in the Tibetan Plateau.

1. Introduction

With the development of exploration and exploitation technology, shale gas, as a clean energy, has become a rising target of natural gas exploration [1–4]. Several sets of organic-matter-rich shale promote the Sichuan Basin as the main exploration area of shale gas in China, which deepens theoretical study of shale gas exploitation [5–8]. In particular, the Wufeng–Longmaxi Formation (WLF) organic-matter-rich shale is widely distributed in the Sichuan Basin, which is the main gas producing formation of several large shale gas fields such as Jiaoshiba, Changning, and Weiyuan (Figure 1) [9–13].

Although the Sichuan Basin experienced multistage tectonic movements [18–25], the Indosinian-Yanshan tectonic deformation was the most important and critically affected shale gas enrichment [26–29]. For example, the wide and gentle structures formed during the tectonic movement generally present favorable preservation conditions for shale gas in the southern Sichuan Basin (Figure 1(c)), including anticlines (e.g., Jiaoshiba, Taiyang-Dazhai, and Dingshan) [14, 16, 30], synclines, or single slopes (e.g., Changning and Weiyuan) [31, 32].

However, there was little report on shale gas in the southwestern Sichuan Basin that shows a similar gas-bearing stratigraphy compared with the southern basin [29, 33]. The first-order geologic difference between the two regions is that the southwestern region has been strongly influenced by the Cenozoic tectonic movement of the Tibetan Plateau, whereas the southern basin has been weakly

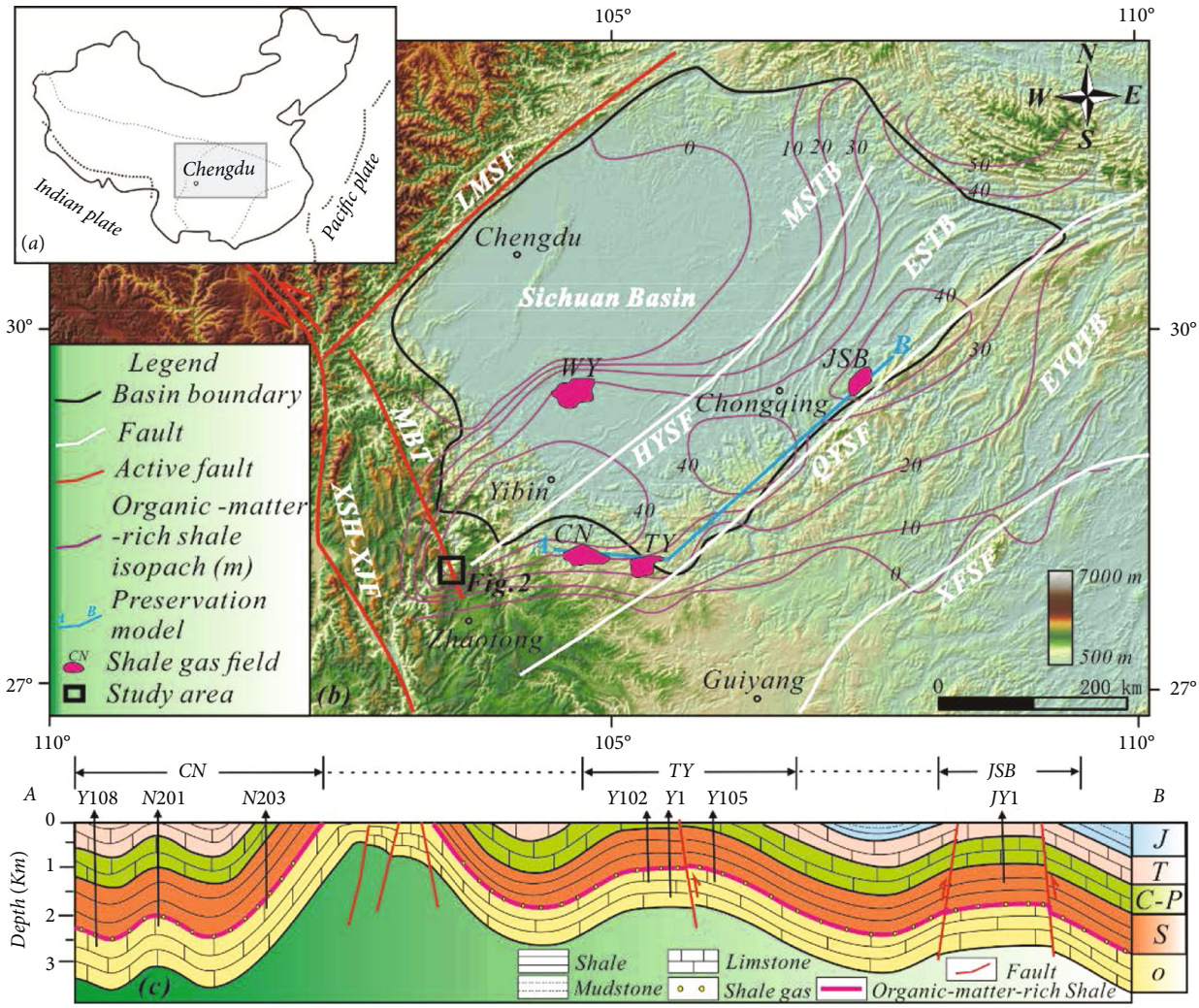

FIGURE 1: Simplified tectonics around the Sichuan Basin and preservation conditions of WLF shale gas. (a) Tectonic location of the Sichuan Basin. (b) The main faults and organic-matter-rich shale isopach contours of WLF around the Sichuan Basin [14, 15]. The Cenozoic Himalayan orogeny resulted in a high topography along the Longmenshan–Xianshuihe–Xiaojiang–Mabian tectonic belts. The low-altitude topography indicates weakly influenced related to the Himalayan movement. Purple lines indicate the organic-matter-rich shale isopach contours of WLF. Commercial shale gas fields with weak Cenozoic deformation are located at the southern Sichuan Basin. (c) Preservation conditions of WLF shale gas in the Changning, Taiyang-Dazhai, and Jiaoshiba shale gas filed [16, 17]. Abbreviation: JSB: Jiaoshiba; WY: Weiyuan; TY: Taiyang-Dazhai; CN: Changning; LMSF: Longenshan fault; XSH-XJF: Xianshuihe-Xiaojiang fault; HYSF: Huayingshan fault; QYSF: Qiyueshan fault; XFSF: Xuefengshan fault; MBF: Mabian fault; MSTB: Middle Sichuan tectonic belt; ESTB: Eastern Sichuan tectonic belt; EYQTB: E-Yu-Qian tectonic belt.

influenced. Although several studies suggested that the Cenozoic tectonic movement may adjust the distribution and accumulation of shale gas in the Tibetan Plateau [28, 34, 35], its detailed mechanism in the southwestern Sichuan Basin is still poorly understood.

Herein, the Mugan area is located at the southwestern region of the Sichuan Basin and shows good shale gas prospects. Although it is not as productive as those large shale gas fields in the southern basin, it provides us an opportunity to further understand the aforementioned issues. Specifically, we analyzed geochemical and physical parameters of five boreholes and tectonic characteristics of two seismic profiles in the Mugan area. We found that three high gas content boreholes are all located within the Mugan syncline (MS) surrounded by some Cenozoic thrust faults, whereas those with poor gas content are located outside the MS, which might be inconsistent to the previous understanding that the Cenozoic tectonic deformation largely destroyed oil and gas preservation conditions. We suggest that some specific structurally stable areas associated with the Cenozoic deformation of the Tibetan Plateau might be favorable for shale gas enrichment, which broadens the limited areas for shale gas exploration in the Sichuan Basin and also may provide new insights for shale gas exploration.

2. Geological Settings

The Mugan area is located at the southwestern Sichuan Basin and the strata range from the upper Proterozoic to the Cenozoic, except for the Carboniferous strata [36]. Uplift

of the Sichuan Basin during the Hercynian period led to the absence of Carboniferous strata throughout the region [9, 37]. Locally, the absence of Devonian strata in the northern Mugan area may be related to Huayingshan fault activity during the Devonian and Carbonian periods [21, 38].

With the NW-trending subduction of the Pacific Plate, a series of NE-SW-trending tectonic belts including E–Yu–Qian tectonic belt, eastern Sichuan tectonic belt, and middle Sichuan tectonic belt in the Yangtze block were gradually formed from south to north during the Indosinian–Yanshanian period (Figures 1(a) and 1(b)) [25, 39]. During this period, folds in the Mugan area were initially formed. Since the Himalayan period, the colliding of the Indian Plate and the Eurasian Plate led to the southeast-ward lateral extrusion of the Tibetan Plateau [40, 41], which is characterized by the Cenozoic tectonic deformation of the Mabian fault (Figure 1(b)) [42–44]. The NS-striking Mabian fault consists of several secondary faults including the Xieziba fault (F_1), Guancun fault (F_2), and Zhongcun fault (F_3). The MS is located between the fault F_1 and F_2 (Figure 2) [45–48]. In general, the Indosinian–Yanshanian and the Himalayan tectonic movement might play an important role in controlling the tectonic development and shale gas preservation in the Mugan area [49, 50].

3. Methods and Data

In order to reveal preservation conditions of shale gas in the Mugan area, we used boreholes and geological profiles to make a detailed interpretation of the seismic profiles and obtained the deep tectonic characteristics of the MS, the Wujiaobao anticline (WA), and the Mabian fault. Specifically, two seismic profiles and five boreholes were conducted during 2016–2018. The seismic profiles were surveyed by an east-west profile AB with 17 km long and a north-south profile CD with 6.2 km long, respectively (Figure 2). BGP Inc., China National Petroleum Corporation (CNPC) collected the original seismic data and processed migration for the stacking velocity to obtain the migration velocity model [51–54]. We used GeoEast and the paradigm for seismic data processing. Seismic interpretation is carried out by identifying key seismic reflectors, which may be continuous or discontinuous [55]. Through the continuous reflectors and logging data, the depth and thickness of the strata can be effectively identified, and the regional structure can be determined [56]. Discontinuities or changes in the number of seismic reflectors are an important basis for speculating faults [57].

In addition, based on the calculation of acoustic and density logging data, we obtained synthetic seismic records, identified the seismic reflectors by combining geological and geophysical data, and finally interpreted the related strata and faults. Moreover, we obtained the time-depth relationship of the seismic profiles according to the five boreholes (D1, D2, D3, X1, andY1) that were drilled through the WLF shale. Based on the above principles, seven seismic reflectors were marked as T_1, T_2, T_3, T_4, T_5, T_6, and T_7, respectively (Figure 3). The geochemical and physical parameters and fractures analysis of the boreholes and loggings are used for interpreting the microstructures and gas-bearing characteristic.

4. Results

4.1. Structural Characteristics within the MS. The seismic profile AB reveals the NS-trending tectonic characteristics of the MS (Figure 4). Combined with boreholes D1 and D2, the reflector T_6 is composed of the Silurian Longmaxi Fm. (S_1l), with a burial depth of 1670–2070 m and a thickness of approximately 400 m. The reflector T_7 is composed of the Ordovician Guanyinqiao Fm. and Cambrian Qiongzhusi Fm. (O_3g-$\in_1q$). The gas-bearing layer is organic-matter-rich shale with a thickness of approximately 35 m. Based on the characteristics of the reflectors, we infer that the central part of the MS is dominated by broad and gentle fold. Moreover, two high-angle concealed faults F4 and F5 can be inferred at the both ends of the profile AB. Although the deformation of the two faults was not intense, displacement of F5 is relatively greater than that of F4. Based on the aforementioned results, we suggest that the NS-trending characteristics of the MS show continuous strata and weak deformation.

The seismic profile CD reveals the EW-trending tectonic characteristics of the MS (Figure 5). The reflectors in the middle part of the profile CD are continuous and smooth, whereas the two ends show complex characteristics. The reflectors revealed by the profile CD fluctuate more intensely than that of the profile AB, some strata are exposed to the surface and eventually taper at the two ends. Based on the profile CD and borehole D2, the seven reflectors are also identified. Moreover, we interpret some faults including F1, F2, and F3, and three concealed faults F6, F7, and F8. Faults F1 and F2 displaced the MS. The east side of the MS shows a steeper dip angle than that of the west side (Figure 5).

4.2. Structural Characteristics at the Periphery of the MS. Two geologic profiles and two boreholes are used to reveal the structural characteristics at Xintan and Yongshan areas in the periphery of the MS. For the Xintan site, the WA is a high-angle northeast-trending fold with a length of approximately 30 km, developed to the northeast side of the MS (Figure 6(a)). The Permian strata are exposed at the core of the WA, whereas the Mesozoic strata are exposed at the two limbs. The strata revealed by borehole X1 are approximately consistent with the regional strata, whereas the Devonian and Carboniferous strata are lacking (Figure 3). The Yongshan site is located to the northwest of MS, which shows a wide gentle syncline that gradually became steep at its eastern limb (Figure 6(b)). The site is lacking the Devonian and Carboniferous strata (Figure 6(b)). Borehole Y1 reveals that thickness of the Permian basalt ($P_3\beta$) is 745 m, which is 400 m greater than other boreholes (Figure 3). Thickness of the WLF shale is 195 m, which is 200 m thinner than the other four boreholes.

4.3. Characteristics of the Shale Gas in the Mugan Area. Gas-bearing characteristics revealed by the five boreholes are

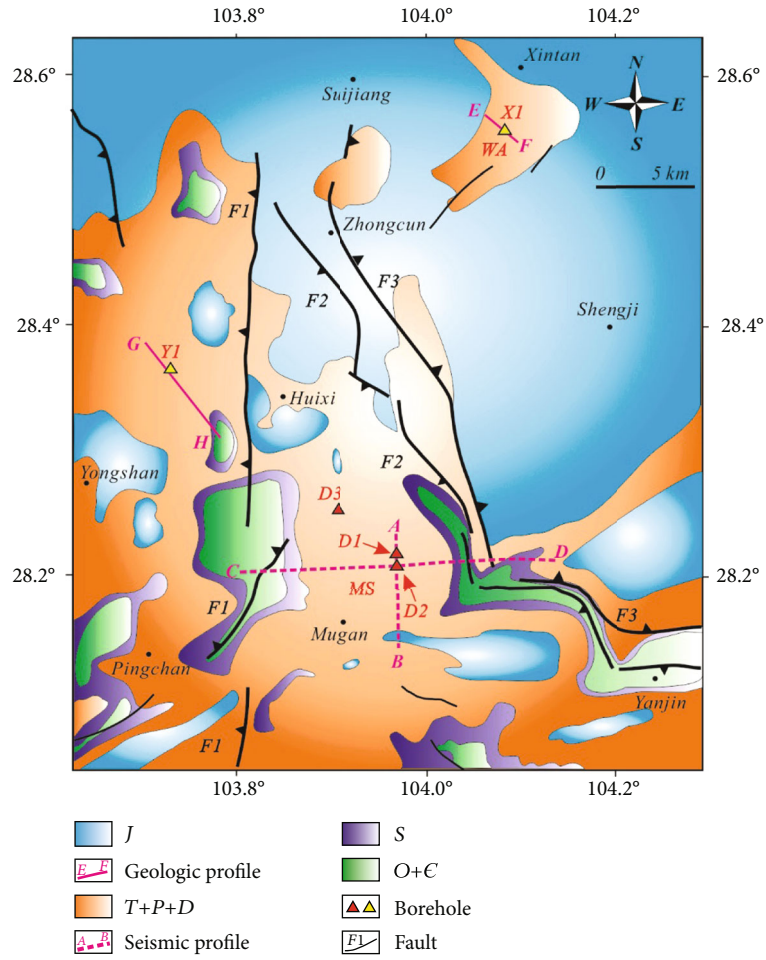

FIGURE 2: Geological map in the Mugan area. The Mabian fault is composed of three branch faults (F1, F2, and F3) with north-south trending. The pre-Silurian strata are exposed on both sides of the MS. Red triangles (D1, D2, and D3) denote boreholes with high gas contents, whereas yellow triangles (X1, Y1) represent boreholes with poor gas contents. Abbreviation: MS: Mugan syncline, WA: Wujiaobao anticline.

different. The boreholes in the MS (D1, D2, and D3) show that the WLF shale has good hydrocarbon generation capacity (Table 1). The average thickness of the organic-matter-rich shale is approximately 35 m. We identified 15 shale gas layers with an average gas content greater than 2.6 m^3/t. The logging and geochemical data reveal that the TOC is greater than 2%. The integrated logging parameters of borehole D1 show a high gas content at depth of 2042-2078 m (Figure 7). In addition, borehole D1 shows that average production of shale gas can be up to 5000 m^3/d after 30 days' trial.

However, boreholes X1 and Y1 located at the periphery of the MS (Figure 2) show relatively poor characteristics. Five discontinuous layers of shale gas were found in the borehole X1 at the depth of 1216.4–1318.8 m. The organic-matter-rich shale is mainly developed at depth of 1289–1308 m with a cumulative thickness of 19 m (Table 1). The organic-matter-rich shale in the borehole X1 can be interpreted by a TOC of 1.66% and an average gas content of 0.61 m^3/t. Similarly, the borehole Y1 reveals that the organic-matter-rich shale is buried at the depth of approximately 1665-1667.5 m with a thickness of 2.75 m, which yields TOC of 1.6% and average gas content of 0.55 m^3/t.

4.4. Physical and Geochemical Characteristics of the Five Cores at the Mugan Area. Fractures in gas-bearing strata can reflect structural preservation conditions [57–59]. According to the spatial characteristics of fractures developed in the organic-matter-rich shale of the five cores, we divide the fractures into two types such as horizontal and oblique to the bedding plane, respectively. Specifically, cores D1, D2, and D3 show 21, 18, and 16 horizontal fractures, whereas cores X1 and Y1 show 22 and 6 horizontal fractures (Table 2). Despite of some uncertainty in identifying horizontal fractures influenced by the bedding planes due to drilling, we suggest that numbers of horizontal fractures are similar for the five cores. Conversely, cores D1, D2, and D3 show 2, 2, and 1 oblique fractures, whereas cores X1 and Y1 show 39 and 11 oblique fractures (Table 2), which indicates that numbers of oblique fractures are much greater at cores X1 and Y1 than that at cores D1, D2, and D3. Moreover, density of oblique fractures is about thirty

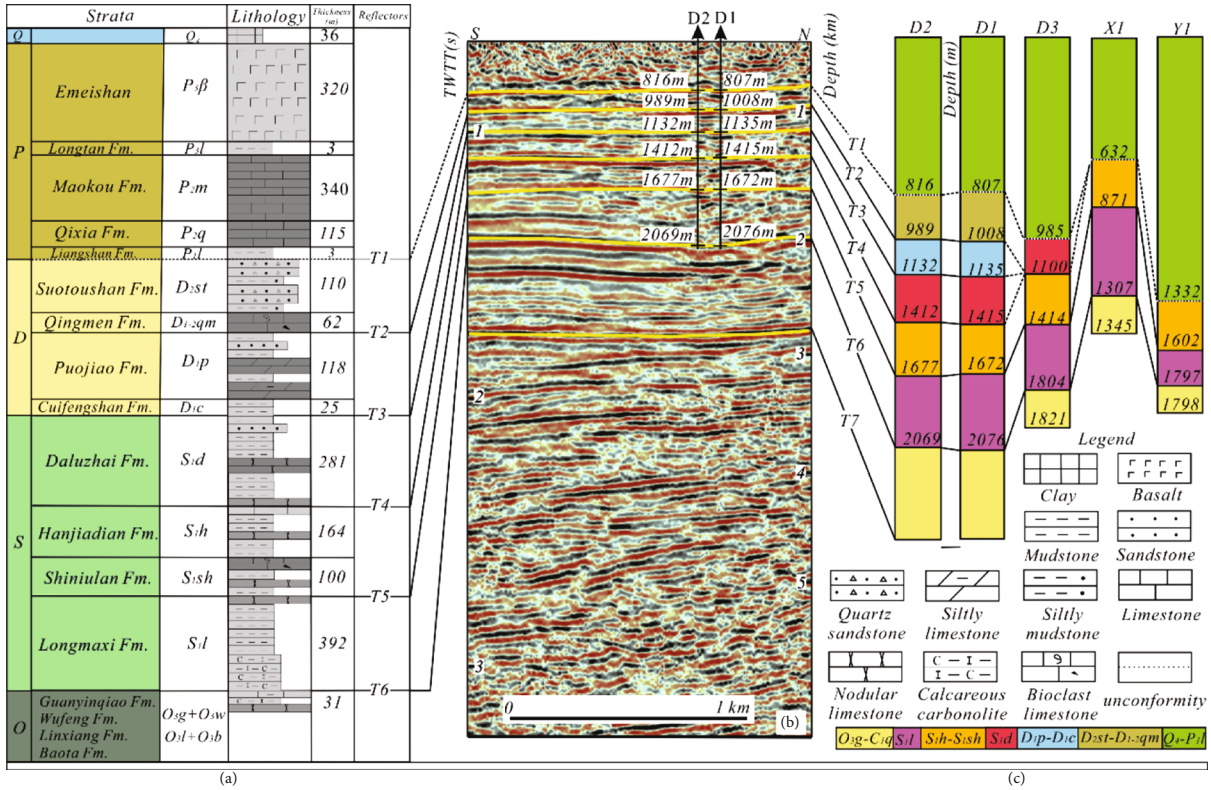

FIGURE 3: Calibration of the seismic reflectors combined with the boreholes. (a) Stratigraphic column. (b) Calibration of the seismic reflectors with boreholes D1 and D2. The calibration profile with time and depth is a part of the seismic profile AB, and the details are shown in Figure 4. TWTT indicates two-way trends (ms). (c) Interpretation of five boreholes (D1, D2, D3, X1, and X2) with reflectors.

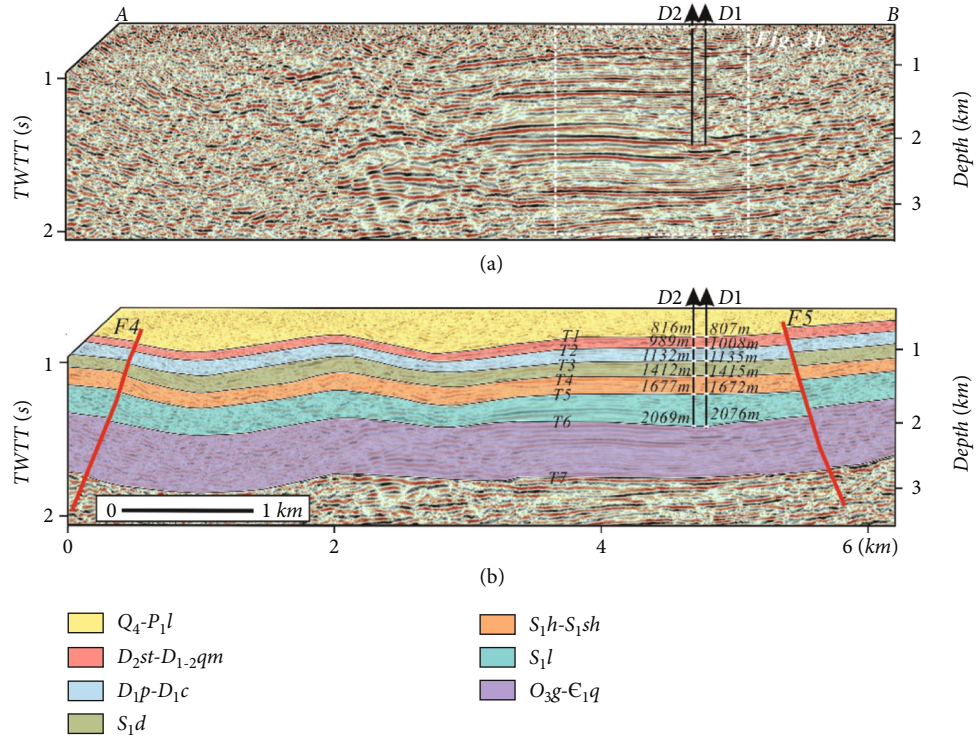

FIGURE 4: Seismic profile AB and its tectonic interpretation. (a) Raw seismic profile AB. The white dashed box correlates to Figure 3. TWTT indicates two-way trends (ms). (b) Tectonic interpretation of the seismic profile AB. Two concealed faults F4 and F5 were identified. D1 and D2 represent boreholes. T1–T7 denote the reflectors.

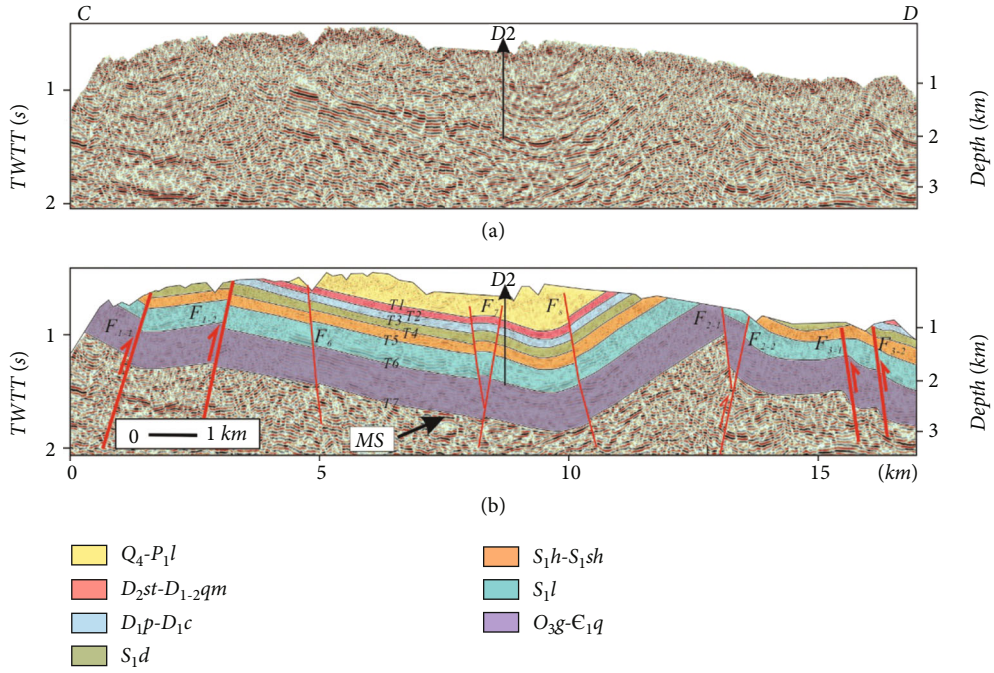

FIGURE 5: Seismic profile CD and its tectonic interpretation. (a) Raw seismic profile CD. TWTT indicates two-way trends (ms). (b) Tectonic interpretation of the seismic profile AB. The MS shows offset by faults inferred from the profile CD. F7 and F8 are concealed faults. Faults F1, F2, and F3 on the profile correspond to Figure 2. D2 represents boreholes. T1–T7 denote the reflectors.

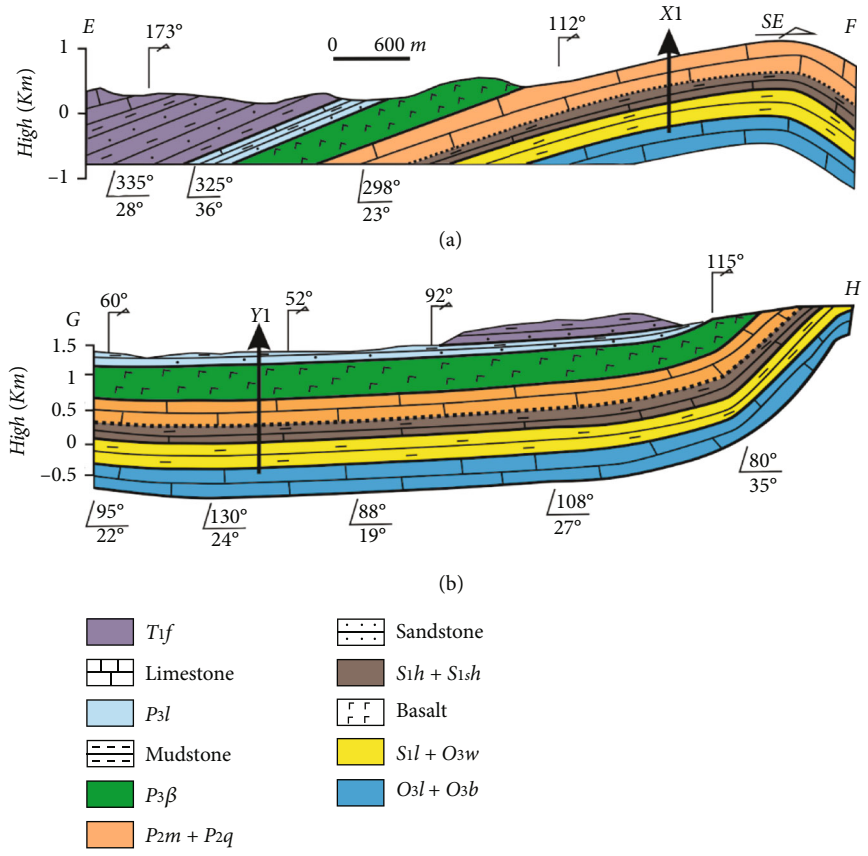

FIGURE 6: Geologic profile EF and GH at Xintan and Yongshan. X1 and Y1 denote boreholes.

Table 1: Comparisons of geochemical parameters in organic-matter-rich shale from shale gas fields in the Sichuan basin.

Strata	S_1l-O_3w						
Borehole	Changning	Taiyang-Dazhai	Mugan syncline			Periphery of Mugan syncline	
	N211 [27]	YS109 [16]	D1	D2	D3	X1	Y1
Samples	/	/	25	24	31	15	8
Thickness of organic-matter-rich shale (m)	31	33	36	33	37	19	2.75
Depth of organic-matter-rich shale (m)	2325-2356	2170-2203	2042-2078	2042-2074	1768-1805	1289-1308	1665-1667.75
TOC (%)	3.7	2.75	2.38	2.32	2.08	1.66	1.6
Ro (%)	2.7	2.9	3.04	3.03	3.04	3.12	3.1
Gas content (m^3/t)	2.17	4.5	3.6	3.5	2.6	0.61	0.55
Comprehensive evaluation	Good			Good		Poor	

Note: the TOC, Ro, and gas content are the average values.

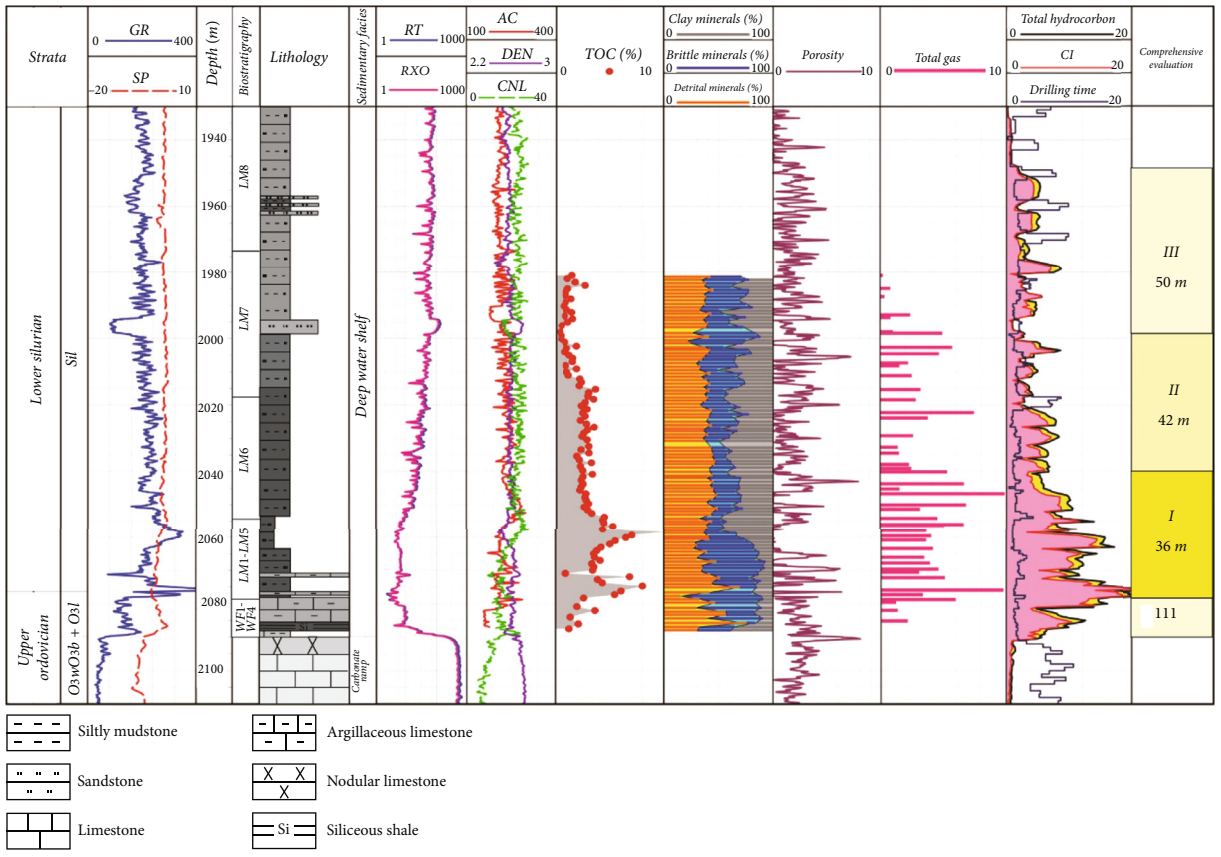

Figure 7: Comprehensive columns of the WLF shale gas revealed in borehole D1. GR in the organic-matter-rich shale is higher than other layers. TOC is 1.43~4.81%, and the high values shown at depth of 2042-2078 m. The gas content and brittleness in this section are also the highest. Obviously, the organic-matter-rich shale of Lower Silurian Longmaxi and Upper Ordovician Wufeng formation is a good material basis for shale gas formation in the Mugan area.

Table 2: Comparisons of fractures revealed though boreholes in the Mugan area.

Borehole	Mugan syncline			Periphery of Mugan syncline	
	D1	D2	D3	X1	Y1
Thickness of organic-matter-rich shale (m)	36	33	37	19	2.75
Horizontal fractures	21	18	16	22	6
Oblique fractures	2	2	1	39	11
Oblique fracture density (/m)	0.06	0.06	0.03	2.1	4

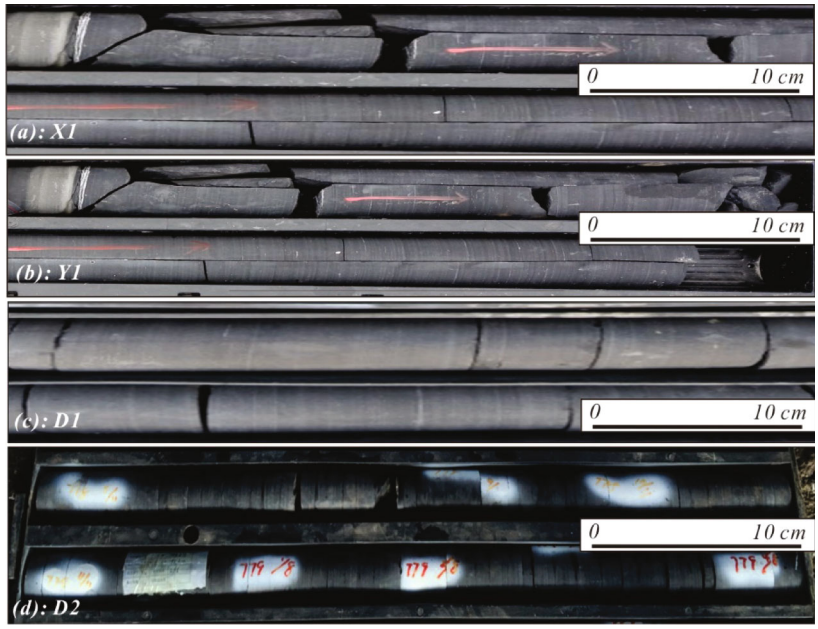

Figure 8: Cores of organic-matter-rich shale (S_1l) in the cores X1, Y1, D1, and D2.

Table 3: Shale parameters of S_1l_1[1].

Borehole	MS			Periphery of MS	
	D1	D2	D3	X1	Y1
Samples	21	23	20	12	10
Helium porosity (%)	8.8	8.5	6.2	—	—
Total pore volume (cm^3/g)	0.0155	0.0146	0.0165	0.0116	0.0114
Total porosity (%)	3.9	3.7	4.3	3.0	2.82
Specific surface area (m^2/g)	25.8	21.7	29.6	20.8	17.5
Average pore diameter (nm)	5.5	5.9	5.0	5.3	4.3
Desorbed gas content (m^3/t)	2.6	2.2	1.6	1.2	0.4
Gas occurrence	Mainly on adsorbed gas	Mainly on adsorbed gas	Mainly on adsorbed gas	Mainly on free gas	Mainly on free gas
Predominant pore type and surface porosity (%)	Organic pore (9.1)	Organic pore (7.9)	Organic pore (9.8)	Dissolved pore (8.2)	Dissolved pore (<1.8)
Organic surface porosity (%)	16.4	15.2	10.5	<1	3.3
Organic pore diameter (μm)	22-293	22-279	22-147	<30	22-62
Distribution characteristics	Honeycomb-like	Honeycomb-like	Homogeneous	Sporadic	Heterogeneous

Multiple parameters of boreholes D1, D2, and D3 in the MS are significantly higher than those in the periphery of MS, such as total pore volume, total sediment content, and specific surface area. Organic surface porosity of boreholes D1, D2, and D3 are higher than 10.5%. At the same time, the desorbed gas content of the MS (>1.6 m^3/t) are higher than that of the periphery (<1.2 m^3/t). Shale with good gas content usually corresponds to evenly distributed pores and high porosity. These parameters may reflect the good reservoir capacity of the MS.

to one hundred times at cores X1 and Y1 than that of cores D1, D2, and D3. The magnitude (length and width) of oblique fractures appears to be much greater in the cores X1 and Y1 than in the cores D1, D2, and D3 (Figure 8). Previous studies suggested that horizontal fractures are mainly related to sliding of regional bedding planes, whereas oblique fractures are associated with regional shearing deformation [60–63]. In other words, oblique fractures rather than horizontal fractures can be more reasonably considered to be a proxy of degrees of regional structural deformation. Therefore, cores X1 and Y1 appear to be more intensely deformed than that of cores D1, D2, and D3.

The pore type and porosity of shale can also reflect structural preservation conditions and formation process of strata [20, 64]. Parameters such as desorbed gas content, organic surface porosity, and organic pore diameter in the MS are all significantly higher than that at the periphery area (Table 3). For example, desorbed gas contents at cores D1, D2, and D3 are ranging from 1.6 to 2.6 m^3/t, whereas the related parameter ranges from 0.4 to 1.2 nd 1.6 to 2.6 m^3/t

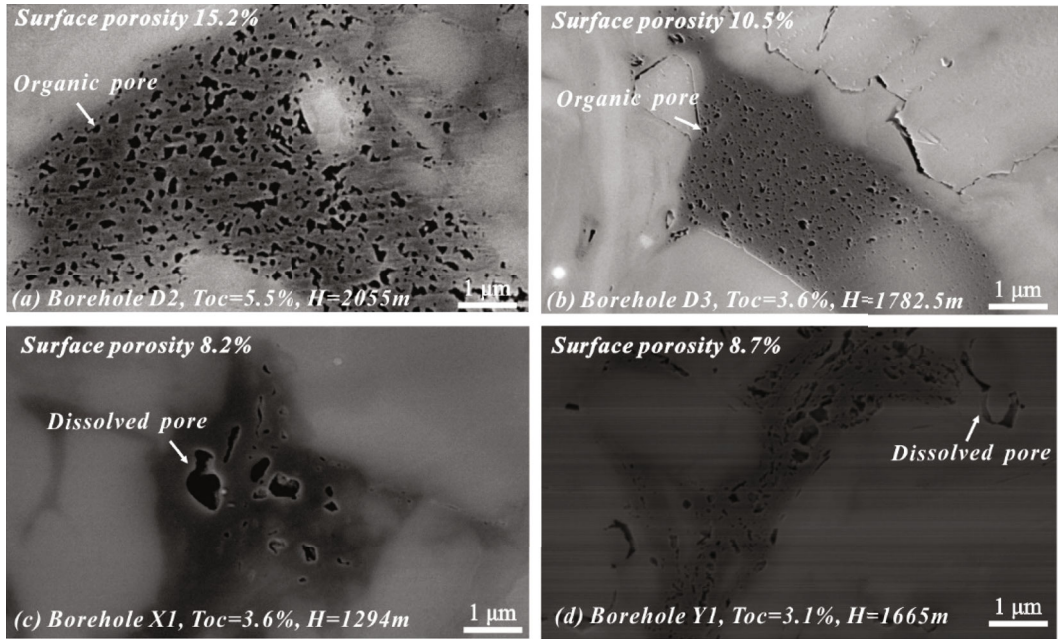

FIGURE 9: Microscopic pores of organic-matter-rich shale from four boreholes. Boreholes D2 (a) and D3 (b) show organic pores with surface porosity at 15.2% and 10.5%. Boreholes X1 (c) and Y1 (d) mainly show dissolved pores with surface porosity at 8.2% and 8.7%.

at cores X1 and Y1. Organic surface porosity at cores D1, D2, and D3 varies between 10.5% and 15.2%, whereas cores X1 and Y1 show <1% and 3.3%, respectively. Organic pore diameter at cores D1, D2, and D3 is 22-293 μm that is greater than that of X1 (<30 μm) and Y1 (22-62 μm). Moreover, pore type of the cores D1, D2, and D3 is mainly organic pore, whereas the cores X1 and Y1 primarily show dissolved pore type (Figure 9 and Table 3). Based on the aforementioned data, it is clear that cores D1, D2, and D3 show a relatively stable unit that favors for better formation of shale gas. However, cores X1 and Y1 indicate intensely deformed unit that destroys formation of shale gas, which result in shale gas to be possibly leaked through dissolved pores. This characteristics of cores X1 and Y1 is also consistent with higher-density oblique fractures, indicating the change of the preservation conditions at the Mugan area.

5. Discussion

5.1. Comparisons of Gas-Bearing Characteristics between the Mugan Area and Southern Sichuan Basin. Gas generation in shale largely determines the gas content, which is primarily affected by the following parameters such as total organic carbon, thermal maturity, kerogen type, mineral composition, and physical parameters [20, 64]. The comparison of multiple parameters shows that the enrichment conditions of shale gas in the MS are similar to those in the southern Sichuan Basin such as Changning (CN) and Taiyang-Dazhai (TY) (Table 1). Specifically, the thickness of the organic-matter-rich shale (upper Ordovician Wufeng–lower Silurian Longmaxi Fm. black shale) in the MS ranges from 33 m to 37 m, which is similar to those in the CN (31 m) and TY (33 m). TOC (2.08%-2.38%) and Ro (3.03%-3.04%) in the MS are similar to those in the CN and TY (2.75%-3.7%, 2.7%-2.9%), respectively. The gas content in the MS (2.6-3.6 m^3/t) is approximately close to that in the CN and TY (2.17-4.5 m^3/t). Moreover, the mineral composition in the MS is basically similar to that in the CN and TY, characterized by the low content of quartz (31.36%) and feldspar (7.5%) and high content of clay (28.8%) and pyrite (2.3%-6.3%) [61]. All the aforementioned parameters indicate that the MS show high gas contents indicative as productive as those large shale gas fields in the southern Sichuan Basin. However, the boreholes in the periphery of the MS shows relatively poor preservation parameters (Table 1). Two boreholes X1 and Y1 show much thinner thickness of organic-matter-rich shale (2.75-19 m), lower TOC (1.6%-1.66%), lower gas content (0.55-0.61 m^3/t), and shallower burial depth (1289-1667.75 m), which indicates that the gas generation processes varied spatially across the Mugan area.

5.2. Shale Gas Preservation in the Mugan Area Related to the Cenozoic Deformation of the Tibetan Plateau. The Indosinian–Yanshanian tectonic movement often produced NE-SW trending structures, while the Himalayan movement produced NS or NW-SE trending structures. Structurally, the Indosinian–Yanshanian tectonic movement produced similar folds in the southwest and southern Sichuan Basin, e.g., anticlines generally exhibit high and steep dip angles, whereas synclines exhibit wide and gentle dip [21, 22, 65, 66]. Although the anticlines in the Mugan area were influenced by fault deformation associated with the Cenozoic tectonic movement, its geometry appears to be consistent with that in the southern Sichuan Basin. Specifically, NS-trending deformation of the MS was relatively weak, only the two ends were deformed by some small concealed faults, indicating that the shale at the NS direction was not destroyed. At the EW direction, the MS shows a gentle shape indicating

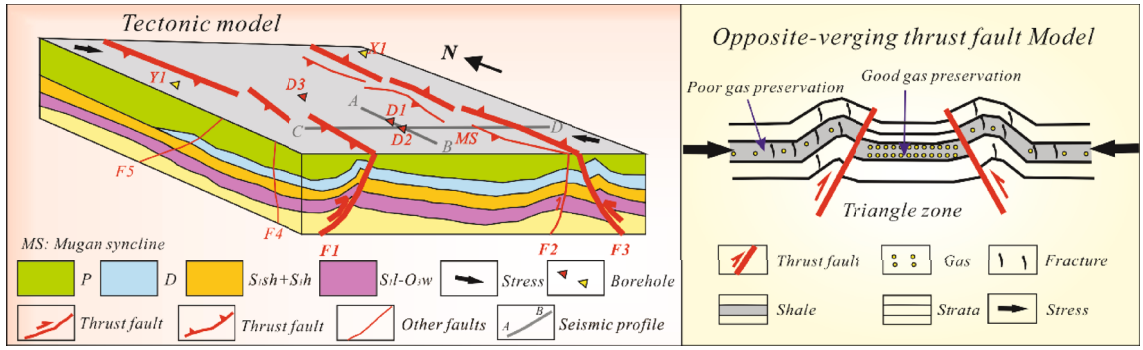

(a) (b)

FIGURE 10: Tectonic and shale gas enrichment model in the Mugan area. (a) Schematic three-dimensional geologic model of the Mugan area. Folds are characterized by high-angle anticlines and wide-gentle synclines. (b) The opposite-verging thrust fault model of the Mugan area. The thrust faults indicate that stress at the hanging wall is relatively concentrated by strong deformation. In other words, the hanging wall produces more fractures and is easily eroded, which results in an unstable cap bedrock. The triangle zone is weakly deformed and shows depositional environment that is favorable for shale gas preservation.

a slightly stronger deformation than its NS direction (Figures 4 and 5). However, most of the faults are small-scaled, concealed, and do not emerge to the surface, which is helpful for shale gas preservation.

Therefore, the Mugan area has the same gas-producing strata and experienced similar fold deformation associated with the Indosinian–Yanshanian tectonic movement, which indicates that the region has a potential shale gas prospect. However, the shale gas contents revealed by the five boreholes in the Mugan area varied spatially as mentioned above, which might imply that deformation associated with the Cenozoic tectonic movement may critically influence shale gas preservation conditions in the Mugan area, we will discuss its mechanism in the following part.

The southern Sichuan Basin has been weakly deformed by the Cenozoic deformation of the Tibetan Plateau, whereas the southwestern region of the basin is at the margin of the Tibetan Plateau and has been strongly influenced by the deformation evidenced by high topography and multiple earthquakes [34, 35]. Specifically, the Mabian fault is a Cenozoic active thrust fault with right-lateral strike slip and is mainly composed of three branch faults (F1, F2, and F3, Figure 10(a)) in the Mugan area [40, 41, 48]. Fault F1 dips westward, indicating that the block on the west side was uplifted and thrusted eastward. The fault F2 is also a westward-dipping fault, but the deformation is much weaker than F1. Fault F3, near F2, dips eastward, indicating that the block on the east wall showed westward thrust deformation. The three branch faults constitute an opposite-verging thrust fault model (Figure 10(b)).

Based on the principles of strain [38, 67–69], the strain in the west hanging wall of F1 is greater than that of the other parts, which indicates that the bedrock in the hanging wall should be more intensely damaged. Furthermore, previous studies suggested that horizontal fractures are mainly related to sliding of regional bedding planes, whereas oblique fractures are associated with regional shearing deformation [16, 28, 70]. In other words, oblique fractures rather than horizontal fractures can be more reasonably considered to be a proxy of degrees of regional deformation. Actually, we found that wide and gentle parts of the MS revealed by D1 and D2 show fewer oblique fractures (1-2/m) (Figures 7(c) and 7(d)), whereas the periphery of MS revealed by X1 and Y1 show multiple oblique fractures (11-39/m) (Figure 8 and Table 2). Moreover, some vertical secondary faults are also observed at borehole Y1 (Figure 8). Numerical studies suggested that shale gas can easily escape through intensely deformed vertical fractures and faults [71, 72], which might be the primary reason for the poor gas content in the borehole X1 and Y1. Therefore, we suggest that the MS can be considered a relatively stable tectonic region.

Secondly, both ends of the MS were uplifted by the opposite-verging thrust faults, which resulted in more erosion in the hanging walls and destroyed shale gas cap rocks. However, the MS is a depositional area in a low strain state that favors shale gas cap rocks to be relatively intact. This model can well explain the differential shale gas preservation status of the five boreholes in the Mugan area, which is also consistent with the classical conclusion that the triangular wedges of the thrust faults are regarded as important oil and gas enrichment areas [73–75].

Thirdly, thrust fault deformation could result in wide-gentle folded strata in the hanging wall to be steeply deformed during the Cenozoic tectonic movement, which is evidenced by the two low gas-bearing boreholes in the high and steep anticlines. For example, borehole X1 is located in the WA characterized with dip angles from 30° to 50°, which implies that the deformation of the WA is much stronger than the MS. Due to the two steep limbs of the anticline, the intense deformation may result in more fractures that are not favorable for shale gas preservation [16, 37]. Therefore, compared with the wide and gentle syncline, the high and steep anticlines with stronger deformation (relatively fractured rocks and steeper strata) are not helpful for shale gas enrichment.

Fourthly, tight strata and thrust faults can effectively prevent shale gas leakage, which is important factor for the preservation of shale gas that is evidenced by the Taiyang-Dazhai gas field and Jiaoshiba gas field [71, 76, 77]. The tight

shale (S_1sh) on the roof and limestone (O_3l) on the floor constitute good sealing layers, the thrust faults play a sealing role, forming a continuous gas reservoir in Taiyang-Dazhai gas field [16, 78]. Similarly, the thrust faults on both sides of the Jiaoshiba area effectively blocked the shale gas in the box-shaped anticline, thus forming a high-yield shale gas field [29, 79–81]. Correspondingly, the sealing effect of strata (S_1sh and O_3l) and thrust faults (F_1 and F_3) in Mugan area is favorable for shale gas enrichment (Figure 10(b)).

5.3. Implications for Shale Gas in the Tibetan Plateau. For the Tibet Plateau, the division of shale gas preservation units should be carried out according to the influence of the Cenozoic movement, which can help us determine specific structurally stable areas for shale gas exploration. The first order of geologic difference between the southwestern and southern Sichuan Basin is the influence of Cenozoic tectonic movement of the Tibetan Plateau. The southern Sichuan Basin is weakly affected by the Cenozoic tectonic movement, whereas its southwest region has been strongly influenced [23, 49, 60, 82, 83]. Numerous studies suggest that wide-gentle folds related to the Indosinian–Yanshanian tectonic movement are helpful for shale gas preservation [49, 77, 84, 85], such as shale gas of the Taiyang-Dazhai gas field and Jiaoshiba gas field is dominantly enriched at wide and gentle anticlines (Figure 1(c)), while shale gas of the Changning gas field is enriched at a low and gentle slope [12, 16, 25, 86–88]. Therefore, the key in shale gas exploration in the southwestern Sichuan Basin is to find an ideal zone similar to the MS in the Mugan area.

Based on the tectonic model in the Mugan area (Figure 10(a)), we suggest that this tectonic localization has well preserved shale gas. Moreover, the pressure coefficients of WLF shale in boreholes D1, D2, and D3 are between 0.8 and 1.0, which are consistent with the normal formation pressure characteristics in the southwestern margin of Sichuan Basin [61]. Therefore, for the southwestern Sichuan Basin, the following ideas may still serve as a reference in the shale gas exploration: first, to determine the existence of an organic-matter-rich shale (such as the WLF shale); second, to trap the gentle part of the strata (such as the Indosinian–Yanshanian movement syncline area); and finally, to trap the good preservation area or areas not affected by Cenozoic structures (such as the Cenozoic fault footwall, a relatively low-strain area). For the sites that meet the above three conditions, the organic-matter-rich shale may be gently developed, with smaller faults or fractures and better cap bedrocks, which can effectively give rise to shale gas enrichment (Figure 10(b)). In other words, tectonic localization may be an important role for future shale gas exploration, which can provide new theoretical insights for shale gas exploration and reduce economic losses caused by uncertainty during the exploration.

6. Conclusion

Through seismic profiles, boreholes, cores, and geological surveys conducted in the Mugan area at the southwestern Sichuan Basin, we found that boreholes D1, D2, and D3 are characterized by high shale gas content, whereas boreholes X1 and Y1 are characterized by poor gas content. By constructing a stratigraphic and tectonic model for the Mugan area, we arrived at the following conclusions. (1) The shale gas exploration in the Mugan area may indicate that strong deformation areas of the Tibetan Plateau have potential for high-yield shale gas. (2) The triangle zone formed by tectonic localization has a low strain, more intact bedrocks, and stable depositional environment that are favorable for local shale gas preservation in the MS. Therefore, trapping the tectonic triangle zone can reduce the geological uncertainty during shale gas exploration in the strong deformation areas of the Tibet Plateau, which might further enrich the shale gas exploration theories and technical ideas.

Data Availability

All the data can be accessible from the corresponding author.

Conflicts of Interest

The authors declare no conflicts of interest.

Acknowledgments

This study is supported by the National Key R&D Program of China (grant 2021YFB2301300), the China Geological Survey Foundation (grants DD20190033 and DD20221635) and the National Natural Science Foundation of China (grant 41804144). Ping Yang, Yuanyuan Sun, and Jianwei Kang are thanked for the helpful scientific discussions.

References

[1] H. Brain and S. Hans-Martin, "Shale gas exploration and exploitation," *Marine and Petroleum. Geology*, vol. 31, no. 1, pp. 1-2, 2012.

[2] B. Selçuk and S. Ikbal, "New horizon in energy: shale gas," *Journal of Natural Gas Science and Engineering*, vol. 35, pp. 637–645, 2016.

[3] W. Zhao, S. C. Zhang, K. He et al., "Origin of conventional and shale gas in Sinian–lower Paleozoic strata in the Sichuan Basin: relayed gas generation from liquid hydrocarbon cracking," *American Association of Petroleum Geologists Bulletin*, vol. 103, no. 6, pp. 1265–1296, 2019.

[4] J. Wei, H. Duan, and Q. Yan, "Shale gas: Will it become a new type of clean energy in China? – A perspective of development potential," *Journal of Cleaner Production*, vol. 294, no. 20, article 126257, 2021.

[5] V. C. Onishi, R. Ruiz-Femenia, R. Salcedo-Díaz et al., "Process optimization for zero-liquid discharge desalination of shale gas flowback water under uncertainty," *Journal of Cleaner Production*, vol. 164, pp. 1219–1238, 2017.

[6] D. Oke, R. Mukherjee, D. Sengupta, T. Majozi, and M. M. El-Halwagi, "Optimization of water-energy nexus in shale gas exploration: from production to transmission," *Energy*, vol. 183, no. 15, pp. 651–669, 2019.

[7] G. M. Sohail, A. E. Radwan, and M. Mahmou, "A review of Pakistani shales for shale gas exploration and comparison

to North American shale plays," *Energy Reports*, vol. 8, pp. 6423–6442, 2022.

[8] S. Sharma, V. Agrawal, and R. N. Akondi, "Role of biogeochemistry in efficient shale oil and gas production," *Fuel*, vol. 259, article 116207, 2020.

[9] D. Oke, R. Mukherjee, D. Sengupta, T. Majozi, and M. M. El-Halwagi, "Factors controlling microfractures in black shale: a case study of Ordovician Wufeng Formation-Silurian Longmaxi Formation in Shuanghe Profile, Changning area, Sichuan Basin, SW China," *Petroleum Exploration and. Development*, vol. 45, no. 5, pp. 818–829, 2018.

[10] C. Potter, "Paleozoic shale gas resources in the Sichuan Basin, China," *American Association of Petroleum Geologists Bulletin*, vol. 102, no. 6, pp. 987–1009, 2018.

[11] C. N. Zou, R. P. Zhu, Z. Chen et al., "Organic-matter-rich shales of China," *Earth-Science Reviews*, vol. 189, pp. 51–78, 2019.

[12] X. S. Guo, Y. Li, T. Borjigen et al., "Hydrocarbon generation and storage mechanisms of deep-water shelf shales of Ordovician Wufeng Formation-Silurian Longmaxi Formation in Sichuan Basin, China," *Petroleum Exploration and Development*, vol. 47, no. 1, pp. 204–213, 2020.

[13] Z. W. Guo, K. Deng, Z. Li et al., *Formation and evolution of Sichuan basin*, China Geology Press, Beijing, China, 1996.

[14] T. L. Guo and H. Zhang, "Formation and enrichment mode of Jiaoshiba shale gas field, Sichuan Basin," *Petroleum Exploration and Development*, vol. 41, no. 1, pp. 31–40, 2014.

[15] B. C. Burchfiel and Z. L. Chen, "Tectonics of the Southeastern Tibetan Plateau and its adjacent foreland," *Geological Society of America Memiors*, vol. 210, pp. 1–231, 2013.

[16] X. Liang, Z. Xu, Z. Zhang et al., "Breakthrough of shallow shale gas exploration in Taiyang anticline area and its significance for resource development in Zhaotong, Yunnan Province, China," *Petroleum Exploration and Development*, vol. 47, no. 1, pp. 12–29, 2020.

[17] C. N. Zou, D. Z. Dong, Y. M. Wang et al., "Shale gas in China: characteristics, challenges and prospects (I)," *Petroleum Exploration and Development*, vol. 42, no. 6, pp. 753–767, 2015.

[18] X. H. Ma and J. Xie, "The progress and prospects of shale gas exploration and development in southern Sichuan Basin, SW China," *Petroleum Exploration and Development*, vol. 45, no. 1, pp. 172–182, 2018.

[19] G. Wang, Z. Jin, G. Liu et al., "Geological implications of gamma ray (GR) anomalies in marine shales: a case study of the Ordovician-Silurian Wufeng-Longmaxi succession in the Sichuan Basin and its periphery, Southwest China," *Journal of Asian Earth Sciences*, vol. 199, article 104359, 2020.

[20] H. Nie, Q. Chen, G. Zhang, C. Sun, P. Wang, and Z. Lu, "An overview of the characteristic of typical Wufeng-Longmaxi shale gas fields in the Sichuan Basin, China," *Natural Gas Industry*, vol. 8, no. 3, pp. 217–230, 2021.

[21] D. P. Yan, M. F. Zhou, H. L. Song, X. W. Wang, and J. Malpas, "Origin and tectonic significance of a Mesozoic multi-layer over-thrust system within the Yangtze Block (South China)," *Tectonophysics*, vol. 361, pp. 239–254, 2003.

[22] D. P. Yan, Z. Bing, M. F. Zhou, G. Wei, H. L. Song, and S. F. Liu, "Constraints on the depth, geometry and kinematics of blind detachment faults provided by fault -propagation folds: an example from the Mesozoic fold belt of South China," *Journal of Structural Geology*, vol. 31, pp. 150–162, 2009.

[23] S. Z. Li, Y. H. Suo, X. Li et al., "Mesozoic tectono-magmatic response in the East Asian ocean-continent connection zone to subduction of the Paleo-Pacific Plate," *Earth-Science Reviews*, vol. 192, pp. 91–137, 2019.

[24] R. Liu, F. Hao, T. Engelder et al., "Stress memory extracted from shale in the vicinity of a fault zone: implications for shale-gas retention," *Marine and Petroleum Geology*, vol. 102, pp. 340–349, 2019.

[25] S. G. Liu, Y. Yang, B. Deng et al., "Tectonic evolution of the Sichuan Basin, Southwest China," *Earth-Science Reviews*, vol. 213, article 103470, 2021.

[26] D. F. Hu, H. Zhang, K. Ni, and G. C. Yu, "Main controlling factors for gas preservation conditions of marine shales in southeastern margins of the Sichuan Basin," *Natural Gas Industry*, vol. 34, no. 6, pp. 17–23, 2014.

[27] H. K. Nie, C. Sun, G. Liu, W. du, and Z. He, "Dissolution pore types of the Wufeng Formation and the Longmaxi Formation in the Sichuan Basin, south China: implications for shale gas enrichment," *Marine and Petroleum Geology*, vol. 101, pp. 243–251, 2019.

[28] Z. L. He, H. K. Nie, S. Li, J. Luo, H. Wang, and G. Zhang, "Differential enrichment of shale gas in upper Ordovician and lower Silurian controlled by the plate tectonics of the Middle-Upper Yangtze, south China," *Marine and Petroleum Geology*, vol. 118, article 104357, 2020.

[29] Y. Fu, Y. Jiang, Q. Hu et al., "Fracturing flowback fluids from shale gas wells in western Chongqing: geochemical analyses and relevance for exploration & development," *Journal of Natural Gas Science and Engineering*, vol. 88, article 103821, 2021.

[30] Z. Lu, Z. He, C. Yu et al., "Characteristics of shale gas enrichment in tectonically complex regions—a case study of the Wufeng-Longmaxi Formations of Lower Paleozoic in southeastern Sichuan Basin," *Oil and Gas Geology*, vol. 42, no. 1, pp. 86–97, 2021.

[31] D. F. He, R. Q. Lu, and H. Huang, "Tectonic and geological setting of the earthquake hazards in the Changning shale gas development zone, Sichuan Basin, SW China," *Petroleum Exploration and Development*, vol. 46, no. 5, pp. 1051–1064, 2019.

[32] W. Guo, J. Tang, J. Ouyang, T. Wang, X. Wang, and Y. Wang, "Characteristics of structural deformation in the southern Sichuan Basin and its relationship with the storage condition of shale gas," *Natural Gas Industry*, vol. 41, no. 5, pp. 11–19, 2021.

[33] X. Chen, J. Fan, Q. Chen, L. Tang, and X. D. Hou, "Toward a stepwise Kwangsian Orogeny," *Science China Earth Science*, vol. 57, no. 3, pp. 379–387, 2014.

[34] C. Z. Jia, B. Li, Y. Lei, and Z. X. Chen, "The structure of Circum-Tibetan Plateau Basin-range system and the large gas provinces," *Science China: Earth Science*, vol. 56, no. 11, pp. 1853–1863, 2013.

[35] C. Z. Jia, C. N. Zou, Z. Yang et al., "Significant progress of continental petroleum geological theory in basins of Central and Western China," *Petroleum Exploration and Development*, vol. 45, no. 4, pp. 573–588, 2018.

[36] Sichuan Geological Bureau, *Regional geological survey report in Leibo*, China Geological Publishing House, 1972.

[37] X. Xu, W. Shi, T. Carr et al., "Mesozoic horizontal stress in the East Sichuan Fold-and-thrust Belt, South China: Insights for Lower Paleozoic shale gas retention," *Journal of Natural*

Gas Science and Engineering, vol. 95, no. 2, article 104154, 2021.

[38] M. Feng and M. An, "Lithospheric structure of the Chinese mainland determined from joint inversion of regional and teleseismic Rayleigh-wave group velocities," *Journal of. Geophysical Research*, vol. 115, no. B6, article B06317, 2010.

[39] X. Chen, J. Fan, Y. Zhang et al., "Subdivision and delineation of the Wufeng and Lungmachi black shales in the subsurface areas of the Yangtze platform," *Journal of Stratigraphy*, vol. 39, no. 4, pp. 351–358, 2015.

[40] Y. F. An, Z. J. Han, and J. Wan, "Research on fission track chronology of Cenozoic uplift in Mabian area, southern Sichuan," *Science China*, vol. 38, no. 5, pp. 555–563, 2008.

[41] Z. J. Han, Y. He, Y. An, and C. Y. Li, "A new seismotectonic Belt: features of the latest structural deformation style in the Mabian Seismotectonic zone," *Acta Geologica Sinica*, vol. 83, no. 1, pp. 218–229, 2009.

[42] Q. D. Deng, *Map of Active Tectonics in China*, Seismological Press, Beijing, China, 2007.

[43] M. K. Bai, M. Chevalier, J. Pan et al., "Southeastward increase of the late Quaternary slip-rate of the Xianshuihe fault, eastern Tibet. Geodynamic and seismic hazard implications," *Earth Planetary and Science Letters*, vol. 485, no. 1, pp. 19–31, 2018.

[44] X. Qiao and Y. Zhou, "Geodetic imaging of shallow creep along the Xianshuihe fault and its frictional properties," *Earth Planetary and Science Letters*, vol. 567, no. 1, article 117001, 2021.

[45] C. Li, D. He, and Y. Sun, "Structural characteristic and origin of intra-continental fold belt in the eastern Sichuan basin, South China block," *Journal of Asian Earth Sciences*, vol. 111, no. 1, pp. 206–221, 2015.

[46] W. G. He, J. Zhou, and K. Yuan, "Deformation evolution of Eastern Sichuan-Xuefeng fold-thrust belt in South China: insights from analogue modelling," *Journal of Structural Geology*, vol. 109, pp. 74–85, 2018.

[47] R. D. Han, "The tectonic pattern and seismic characteristic of Mabian-Yongshan seismic zone," *Seismic and Geology*, vol. 15, no. 3, pp. 253–260, 1993.

[48] X. Liu, S. Zhang, G. Su, and Q. L. Guo, "Late quaternary feature of the central part of the Yingjing-Mabian-Yanjin fault zone, Sichuan province," *Memoir Of Crustal Tectonics and Tectonic Stress*, vol. 16, pp. 30–37, 2003.

[49] J. Wu, C. Liang, Z. Hu et al., "Sedimentation mechanisms and enrichment of organic matter in the Ordovician Wufeng Formation-Silurian Longmaxi Formation in the Sichuan Basin," *Marine and Petroleum Geology*, vol. 101, pp. 556–565, 2019.

[50] Q. Y. Gou, S. Xu, F. Hao, Z. Shu, and Z. Zhang, "Making sense of micro-fractures to the Longmaxi shale reservoir quality in the Jiaoshiba area, Sichuan Basin, China: implications for the accumulation of shale gas," *Journal of Natural Gas Science and Engineering*, vol. 94, article 104107, 2021.

[51] J. F. Claerbout, *Imagination of the Earth's Interior*, Blackwell Scientific Publication, 1985.

[52] Z. Yilmaz, *Seismic data analysis: processing, inversion, and interpretation of seismic data*, Society of Exploration Geophysicists, 2001.

[53] D. Motta, J. Abad, E. Langendoen, and M. H. Garcia, "A simplified 2D model for meander migration with physically-based bank evolution," *Geomorphology*, vol. 163-164, pp. 10–25, 2012.

[54] H. Zhou, H. Hu, Z. Zou, Y. Wo, and O. Youn, "Reverse time migration: a prospect of seismic imaging methodology," *Earth-Science Reviews*, vol. 179, pp. 207–227, 2018.

[55] H. W. Posamentier, V. Paumard, and S. C. Lang, "Principles of seismic stratigraphy and seismic geomorphology I: extracting geologic insights from seismic data," *Earth-Science Reviews*, vol. 228, article 103963, 2022.

[56] P. M. Burgess, P. Winefield, M. Minzoni, and C. Elders, "Methods for identification of isolated carbonate buildups from seismic reflection data," *The American Association of Petroleum Geologists Bulletin*, vol. 97, no. 7, pp. 1071–1098, 2013.

[57] A. P. Bischoff, A. Nicol, and M. Beggs, "Stratigraphy of architectural elements in a buried volcanic system and implications for hydrocarbon exploration," *Interpretation*, vol. 5, pp. 141–159, 2017.

[58] Q. Feng, N. Qiu, X. Fu et al., "Permian geothermal units in the Sichuan Basin: implications for the thermal effect of the Emeishan mantle plume," *Marine and Petroleum Geology*, vol. 132, article 105226, 2021.

[59] B. He, Y. G. Xu, S. L. Chung, L. Xiao, and Y. Wang, "Sedimentary evidence for a rapid, kilometer-scale crustal doming prior to the eruption of the Emeishan flood basalts," *Earth Planetary and Science Letters*, vol. 213, no. 3-4, pp. 391–405, 2003.

[60] S. Xu, Q. Y. Gou, F. Hao et al., "Shale pore structure characteristics of the high and low productivity wells, Jiaoshiba shale gas field, Sichuan Basin, China: dominated by lithofacies or preservation condition?," *Marine and Petroleum Geology*, vol. 114, article 104211, 2020.

[61] P. Yang, Z. Wang, Q. Yu et al., "Evaluation of shale gas potential in Ordovician Wufeng-Silurian Longmaxi formations, Mugan syncline, northeastern Yunnan," *Petroleum Geology and Experiment*, vol. 41, no. 5, pp. 638–647, 2019.

[62] D. Zhang, Q. Yu, J. Lu et al., "Graptolite biozonation of the Wufeng and Lungmachi formations and its environmental implication from the Xindi 2 borehole in Yongshan–Mugan area, NE Yunnan," *Earth Science*, vol. 45, no. 3, pp. 739–751, 2019.

[63] C. R. Clarkson, N. Solano, R. M. Bustin et al., "Pore structure characterization of North American shale gas reservoirs using USANS/SANS, gas adsorption, and mercury intrusion," *Fuel*, vol. 103, pp. 606–616, 2013.

[64] J. Zhang, S. Liu, X. Wei, X. Tang, and Y. Liu, "Evaluation of gas content in shale," *Oil and Gas Geology*, vol. 42, no. 1, pp. 28–40, 2021.

[65] Z. Wang, J. Zhang, T. Li, G. Xie, and Z. Ma, "Structural analysis of the multi-layer detachment folding in eastern Sichuan province," *Acta Geologica Sinica*, vol. 84, no. 3, pp. 497–514, 2010.

[66] Y. Li, M. Li, J. Zhang et al., "Influence of the Emeishan basalt eruption on shale gas enrichment: a case study of shale from Wufeng-Longmaxi formations in northern Yunnan and Guizhou provinces," *Fuel*, vol. 282, no. 3, article 118835, 2020.

[67] K. Zhang, C. Jia, Y. Song et al., "Analysis of Lower Cambrian shale gas composition, source and accumulation pattern in different tectonic backgrounds: a case study of Weiyuan Block in the Upper Yangtze region and Xiuwu Basin in the Lower Yangtze region," *Fuel*, vol. 263, no. 1, article 115978, 2020.

[68] S. M. Zhang, G. Z. Nie, X. D. Liu, J. J. Ren, and G. Su, "Kinematical and structural patterns of Yingjing-Mabian-Yanjin thrust fault zone, southeast of Tibetan plateau, and its

segmentation from earthquakes," *Seismic Geology*, vol. 27, no. 2, pp. 221–233, 2005.

[69] S. Xu, Q. Gou, F. Hao, B. Zhang, Z. Shu, and Y. Zhang, "Multiscale faults and fractures characterization and their effects on shale gas accumulation in the Jiaoshiba area, Sichuan Basin, China," *Journal of Petroleum Science and Engineering*, vol. 189, article 107026, 2020.

[70] J. Z. Li, D. H. Li, D. Z. Dong, and S. J. Wang, "Comparison and enlightenment on formation condition and distribution characteristics of shale gas between China and US," *Chinese Engineering Science*, vol. 14, no. 6, pp. 56–63, 2012.

[71] Z. Xu, X. Liang, H. Lu et al., "Structural deformation characteristics and shale gas preservation conditions in the Zhaotong National Shale Gas Demonstration Area along the southern margin of the Sichuan Basin," *Natural Gas Industry*, vol. 7, no. 3, pp. 224–233, 2020.

[72] R. Wang, W. Ding, Y. Zhang et al., "Analysis of developmental characteristics and dominant factors of fractures in Lower Cambrian marine shale reservoirs: a case study of Niutitang formation in Cen'gong block, southern China," *Journal of Petroleum Science and Engineering*, vol. 138, pp. 31–49, 2016.

[73] P. G. Buchanan and K. R. McClay, "Sandbox experiments of inverted listric and planar fault systems," *Tectonophysics*, vol. 188, no. 1-2, pp. 97–115, 1991.

[74] A. Rotevatn and D. Peacock, "Strike-slip reactivation of segmented normal faults: implications for basin structure and fluid flow," *Basin Research*, vol. 30, no. 6, pp. 1264–1279, 2018.

[75] H. Burgin, P. Robion, and K. Amrouch, "Layer parallel stretching? Characterising magnetic and pore-fabric styles at a rifted continental margin: New insights from the Otway Ranges, Australia," *Tectonophysics*, vol. 815, no. 20, article 228975, 2021.

[76] Y. Wang, S. Xu, F. Hao et al., "Geochemical and petrographic characteristics of Wufeng-Longmaxi shales, Jiaoshiba area, southwest China: Implications for organic matter differential accumulation," *Marine and Petroleum Geology*, vol. 102, pp. 138–154, 2019.

[77] Z. Jin, H. K. Nie, Q. Liu, J. Zhao, and T. Jiang, "Source and seal coupling mechanism for shale gas enrichment in upper Ordovician Wufeng Formation - Lower Silurian Longmaxi Formation in Sichuan Basin and its periphery," *Marine and Petroleum Geology*, vol. 97, pp. 78–93, 2018.

[78] S. Chen, Y. Zhu, S. Chen, H. Yufu, F. Changqing, and F. Junhua, "Hydrocarbon generation and shale gas accumulation in the Longmaxi formation, southern Sichuan Basin, China," *Marine and Petroleum Geology*, vol. 86, pp. 248–258, 2017.

[79] X. S. Guo, D. F. Hu, Y. Li, W. Zhihong, W. Xiangfeng, and L. Zhujiang, "Geological factors controlling shale gas enrichment and high production in Fuling shale gas field," *Petroleum Exploration and. Development*, vol. 44, no. 4, pp. 513–523, 2017.

[80] W. Liu, J. Wu, H. Jiang et al., "Cenozoic exhumation and shale-gas enrichment of the Wufeng-Longmaxi formation in the southern Sichuan basin, western China," *Marine and Petroleum Geology*, vol. 125, article 104865, 2021.

[81] Z. Qiu and C. Zou, "Controlling factors on the formation and distribution of "sweet-spot areas" of marine gas shales in South China and a preliminary discussion on unconventional petroleum sedimentology," *Journal of Asian Earth Sciences*, vol. 194, no. 1, article 103989, 2020.

[82] N. J. Richardson, A. L. Densmore, D. Seward et al., "Extraordinary denudation in the Sichuan Basin: insights from low-temperature thermochronology adjacent to the eastern margin of the Tibetan Plateau," *Journal of Geophysical Research*, vol. 113, no. B4, article B04409, 2008.

[83] Y. T. Tian, B. Kohn, N. S. Qiu et al., "Eocene to Miocene out-of-sequence deformation in the eastern Tibetan Plateau: insights from shortening structures in the Sichuan basin," *Journal of Geophysical research: Solid Earth*, vol. 123, no. 2, pp. 1840–1855, 2018.

[84] E. Wang, B. C. Burchfiel, L. H. Royden et al., "Late Cenozoic Xianshuihe-Xiaojiang, red river, and Dali fault systems of southwestern Sichuan and central Yunnan, China," *Geological Society of America: Special Papers*, vol. 327, pp. 1–108, 1998.

[85] E. Wang, K. Meng, Z. Su et al., "Block rotation: tectonic response of the Sichuan basin to the southeastward growth of the Tibetan Plateau along the Xianshuihe-Xiaojiang fault," *Tectonics*, vol. 33, no. 5, pp. 686–718, 2014.

[86] A. Yin and T. M. Harrison, "Geologic evolution of the Himalayan-Tibetan orogen," *Annual Review of Earth and Planetary Sciences*, vol. 28, no. 1, pp. 211–280, 2000.

[87] E. Mohammadian, B. Liu, and A. Riazi, "Evaluation of different machine learning frameworks to estimate CO2 solubility in NaCl brines: implications for CO_2 injection into low-salinity formations," *Lithosphere*, vol. 2022, no. Special 12, 2022.

[88] H. B. Wang, T. Zhou, and F. X. Li, "A new approach for automatic optimization of complex fracture network in shale reservoirs," *Lithosphere*, vol. 2021, no. Special 1, 2021.